

## SPECTROSCOPIC CONFIRMATION OF TWO MASSIVE RED-SEQUENCE-SELECTED GALAXY CLUSTERS AT $z \sim 1.2$ IN THE SPARCS-NORTH CLUSTER SURVEY

ADAM MUZZIN<sup>1</sup>, GILLIAN WILSON<sup>2</sup>, H.K.C. YEE<sup>3</sup>, HENK HOEKSTRA<sup>4,5,6</sup>, DAVID GILBANK<sup>7</sup>, JASON SURACE<sup>8</sup>, MARK LACY<sup>8</sup>, KRIS BLINDERT<sup>9</sup>, SUBHABRATA MAJUMDAR<sup>10</sup>, RICARDO DEMARCO<sup>2</sup>, JONATHAN P. GARDNER<sup>11</sup>, MIKE GLADDERS<sup>12</sup> & CAROL LONSDALE<sup>13</sup>

*Draft version October 29, 2018*

### ABSTRACT

The Spitzer Adaptation of the Red-sequence Cluster Survey (SpARCS) is a deep  $z'$ -band imaging survey covering the *Spitzer* SWIRE Legacy fields designed to create the first large homogeneously-selected sample of massive clusters at  $z > 1$  using an infrared adaptation of the cluster red-sequence method. We present an overview of the northern component of the survey which has been observed with CFHT/MegaCam and covers 28.3 deg<sup>2</sup>. The southern component of the survey was observed with CTIO/MOSAICII, covers 13.6 deg<sup>2</sup>, and is summarized in a companion paper by Wilson et al. (2008). We also present spectroscopic confirmation of two rich cluster candidates at  $z \sim 1.2$ . Based on Nod-and-Shuffle spectroscopy from GMOS-N on Gemini there are 17 and 28 confirmed cluster members in SpARCS J163435+402151 and SpARCS J163852+403843 which have spectroscopic redshifts of 1.1798 and 1.1963, respectively. The clusters have velocity dispersions of  $490 \pm 140$  km/s and  $650 \pm 160$  km/s, respectively which imply masses ( $M_{200}$ ) of  $(1.0 \pm 0.9) \times 10^{14} M_{\odot}$  and  $(2.4 \pm 1.8) \times 10^{14} M_{\odot}$ . Confirmation of these candidates as *bonafide* massive clusters demonstrates that two-filter imaging is an effective, yet observationally efficient, method for selecting clusters at  $z > 1$ .

*Subject headings:* infrared: galaxies

### 1. INTRODUCTION

In the nearby universe there are numerous lines of evidence suggesting that environmental processes could be the dominant force driving the evolution of the galaxy population. Properties such as star formation rate (SFR, e.g., Lewis et al. 2002; Gomez et al. 2003; Kauffmann et al. 2004), morphology (e.g., Dressler 1980; Goto et al. 2003; Park et al. 2007), stellar mass (e.g., Kauffmann et al. 2004), color (e.g., Hogg et al. 2003; Balogh et al. 2004; Blanton et al. 2005), and luminosity (e.g., Croton et al. 2005; Park et al. 2007) are all strongly correlated with local galaxy density. Although there is still debate

about which, if any, of these relations are “fundamental” (e.g., Hogg et al. 2004; Park et al. 2007), it is clear that the mean properties of galaxies we measure depend strongly on the type of environment they occupy.

An obvious first step toward a better understanding of environmental processes is to study how they evolve with redshift. At higher redshift, the overall population of galaxies is younger and have been living within their local environment for less time. The environmental processes that are most effective and have the shortest timescales should be most apparent when comparing galaxies at different densities in the high redshift universe. The data at higher redshift are still somewhat sparse compared to the nearby universe but it is beginning to emerge that properties such as the SFR (e.g., Elbaz et al. 2007; Cooper et al. 2008; Poggianti et al. 2008), color (e.g., Cooper et al. 2007) and morphology (e.g., Dressler et al. 1997; Postman et al. 2005; Smith et al. 2005, Capak et al. 2007) are still correlated with local density, albeit differently from the nearby universe.

Of particular interest for understanding environmental processes are the cores of rich galaxy clusters. These are the most extreme density environments at all redshifts, and if environment is truly an important force in galaxy evolution a comparison of the properties of galaxies that live in this environment to those that live in the field should provide the largest contrasts. Despite their potential value for such studies, and the abundance of resources directed at finding distant clusters, there are still relatively few confirmed rich clusters at  $z > 1$ .

The major challenge for cluster surveys targeting the  $z > 1$  range is the need to be simultaneously deep enough to detect either the galaxies or hot X-ray gas in clusters and yet wide enough to be able to cover a large area because of the rarity of rich clusters at  $z > 1$ . The require-

<sup>1</sup> Department of Astronomy, Yale University, New Haven, CT, 06520-8101; adam.muzzin@yale.edu

<sup>2</sup> Department of Physics and Astronomy, University of California, Riverside, CA 92521

<sup>3</sup> Department of Astronomy & Astrophysics, University of Toronto, 50 St. George St., Toronto, Ontario, Canada, M5S 3H4

<sup>4</sup> Department of Physics and Astronomy, University of Victoria, Victoria, BC V8P 5C2, Canada

<sup>5</sup> Alfred P. Sloan Fellow

<sup>6</sup> Leiden Observatory, Leiden University, PO Box 9513, 2300RA Leiden, The Netherlands

<sup>7</sup> Astrophysics and Gravitation Group, Department of Physics & Astronomy, University of Waterloo, Waterloo, Ontario, Canada N2L 3G1

<sup>8</sup> Spitzer Science Center, California Institute of Technology, 220-6, Pasadena, CA, 91125

<sup>9</sup> Max Planck Institute for Astronomy Koenigstuhl 17, 69117, Heidelberg, Germany

<sup>10</sup> Department of Astronomy and Astrophysics, Tata Institute of Fundamental Research 1, Homi Bhabha Road, Colaba, Mumbai 400 005, India

<sup>11</sup> Goddard Space Flight Center, Code 665, Laboratory for Observational Cosmology, Greenbelt MD 20771

<sup>12</sup> University of Chicago, 5640 South Ellis Avenue, Chicago, IL 60637

<sup>13</sup> North American ALMA Science Center, NRAO Headquarters, 520 Edgemont Road, Charlottesville, VA 22903

ment of both depth and area has pushed X-ray detection of clusters with current telescopes to the limit.

The largest area targeted X-ray cluster surveys are the XMM-LSS (Valtchanov et al. 2004; Andreon et al. 2005; Pierre et al. 2006) and the XMM-COSMOS (Finoguenov et al. 2007), and while these have been successful at discovering  $z > 1$  clusters (e.g., Bremer et al. 2006), they cover areas of only 9 and 2 deg<sup>2</sup>, respectively and are therefore limited to fairly low mass systems on average. Indeed, X-ray detection of clusters at  $z > 1$  is so challenging that currently the most promising surveys are those searching for clusters serendipitously in the *entire* XMM-Newton archive (e.g., Romer et al. 2001; Mullis et al. 2005; Stanford et al. 2006; Lamer et al. 2008).

Complementary to X-ray detection is optical detection of clusters using overdensities of galaxies selected using the red-sequence (e.g., Gladders & Yee 2000, 2005; Gilbank et al. 2004; Muzzin et al. 2008) or photometric redshifts (e.g., Stanford et al. 2005; van Breuklen et al. 2007; Eisenhardt et al. 2008). Recently, it has become clear that the key to discovering clusters above  $z > 1$  with these techniques is the incorporation of infrared (IR) data which probes the peak of the stellar emission for galaxies at  $z > 1$ .

Although IR surveys have thus far been confined to modest areas (ranging from 0.5 - 8.5 deg<sup>2</sup>) they have been extremely successful at detecting  $z > 1$  clusters (e.g., Stanford et al. 2005; Brodwin et al. 2006; van Breuklen et al. 2007; Zatloukal et al. 2007; Krick et al. 2008; Eisenhardt et al. 2008; Muzzin et al. 2008). The IR cluster community is now regularly discovering clusters at  $z > 1$  and shortly IR-detected clusters should outnumber their X-ray counterparts.

Currently the largest area IR survey still deep enough to detect clusters at  $z > 1$  is the *Spitzer* Wide-Area Infrared Extragalactic Survey (SWIRE, Lonsdale et al. 2003; Surace et al. 2005). SWIRE covers  $\sim 50$  deg<sup>2</sup> in the *Spitzer* bandpasses and is slightly deeper, and nearly a factor of six larger than the next largest IR cluster survey, the IRAC Shallow Survey Cluster Search (ISCS, Eisenhardt et al. 2008).

In Muzzin et al. (2008) we demonstrated the potential of using the red-sequence method with *Spitzer* data to detect distant clusters using data from the 3.8 deg<sup>2</sup> *Spitzer* First Look Survey (FLS, Lacy et al. 2004). In 2006 we began observations for the *Spitzer* Adaptation of the Red-sequence Cluster Survey (SpARCS), a deep  $z'$ -band imaging survey of the SWIRE fields. SpARCS aims to discover the first large, yet homogeneously-selected sample of rich clusters at  $z > 1$  using the red-sequence method. SpARCS is similar to the RCS surveys (Gladders & Yee 2005; Yee et al. 2007) which target clusters to  $z \sim 1$  using an R -  $z'$  color except that we use a  $z' - 3.6\mu\text{m}$  color, which spans the 4000Å break at  $z > 1$ . With a total area effective area of 41.9 deg<sup>2</sup> SpARCS is currently the only  $z > 1$  cluster survey that can discover a significant number of rare rich clusters. These clusters will be extremely valuable for quantifying the evolution of galaxy properties in the densest environments at high redshift.

This paper is organized as follows. In § 2 we provide a brief overview of the northern component of the SpARCS survey (the southern component is summarized in Wil-

son et al. 2008). In § 3 we discuss the selection of cluster candidates that were chosen for followup spectroscopy, and in § 4 we present spectroscopic confirmation of two  $z > 1$  clusters from early SpARCS data. In § 5 we present the dynamical analysis of the clusters followed by a discussion of the cluster properties in § 6. We conclude with a summary in § 7.

Throughout this paper we assume an  $\Omega_m = 0.3$ ,  $\Omega_\Lambda = 0.7$ ,  $H_0 = 70 \text{ km s}^{-1} \text{ Mpc}^{-1}$  cosmology. All magnitudes are on the Vega system unless indicated otherwise.

## 2. THE SPARCS-NORTH SURVEY

The SWIRE survey is located in six fields and contains  $\sim 50$  deg<sup>2</sup> of imaging in the four IRAC bandpasses (3.6 $\mu\text{m}$ , 4.5 $\mu\text{m}$ , 5.8 $\mu\text{m}$ , and 8.0 $\mu\text{m}$ ) and the three MIPS bandpasses (24 $\mu\text{m}$ , 70 $\mu\text{m}$ , and 160 $\mu\text{m}$ ). Three of the fields are located in the northern hemisphere (ELAIS-N1, ELAIS-N2, and the Lockman Hole), two of the fields are located in the southern hemisphere (ELAIS-S1, and the Chandra-S), and one of the fields is equatorial, the XMM-LSS field. A thorough discussion of the data reduction, photometry, cluster finding, and the SpARCS catalogue for all fields will be presented in a future paper by A. Muzzin et al. (2009, in preparation). Here we present a brief summary of the  $z'$ -band observations of the ELAIS-N1, ELAIS-N2, Lockman Hole, and XMM-LSS<sup>14</sup> fields obtained with CFHT/MegaCam; hereafter the SpARCS-North Survey. Observations of the ELAIS-S1 and Chandra-S fields were obtained with the CTIO/MOSAICII and are outlined in the companion paper by Wilson et al. (2008).

The IRAC imaging of the ELAIS-N1, ELAIS-N2, Lockman, and XMM-LSS fields covers areas of 9.8, 4.5, 11.6, and 9.4 deg<sup>2</sup>, respectively. In Figure 1 we plot the IRAC 3.6 $\mu\text{m}$  mosaics for these fields. The superposed white squares represent the locations of the CFHT/MegaCam pointings. The pointings were designed to maximize the overlap with the IRAC data, but to minimize the overall number of pointings by omitting regions that have little overlap with the IRAC data. There are a total of 12, 5, 15, and 13 MegaCam pointings in the ELAIS-N1, ELAIS-N2, Lockman Hole and XMM-LSS fields, respectively.

We obtained observations in the  $z'$ -band with 6000s of integration time for each pointing in the ELAIS-N1, ELAIS-N2 and Lockman Hole fields in queue mode using CFHT/MegaCam which is composed of 36 4096  $\times$  2048 pixel CCDs, and has a field of view (FOV) of  $\sim 1$  deg<sup>2</sup>. Omitting the large chip gap areas and regions contaminated by bright stars, the total overlap region with both  $z'$  and IRAC data is 28.3 deg<sup>2</sup>.

Photometry was performed on both the  $z'$  and IRAC mosaics using the SExtractor photometry package (Bertin & Arnouts 1996). Colors were determined using 3 IRAC pixel (3.66 $''$ ) diameter apertures. The IRAC data was corrected for flux lost outside this aperture due to the wings of the PSF using aperture corrections measured by Lacy et al. (2005). Total magnitudes for the IRAC photometry were computed using the method outlined in Lacy et al. (2005) and Muzzin et al. (2008). The  $5\sigma$  depth of the  $z'$  data varies depending on the seeing

<sup>14</sup> The XMM-LSS data was obtained as part of the CFHT Legacy Survey

and the sky background; however, the mean  $5\sigma$  depth for extended sources is  $z' \sim 23.7$  Vega (24.2 AB).

### 3. CLUSTER SELECTION

Clusters are found in the data using the cluster red-sequence algorithm developed by Gladders & Yee (2000; 2005). Muzzin et al. (2008) used a slightly modified version of the algorithm to detect clusters at  $0 < z < 1.3$  in the FLS using an R -  $3.6\mu\text{m}$  color. We use the Muzzin et al. (2008) code for the SpARCS data. The change from a R -  $3.6\mu\text{m}$  color to a  $z' - 3.6\mu\text{m}$  is optimum for targeting clusters at  $z > 1$ , where the  $z' - 3.6\mu\text{m}$  color spans the  $4000\text{\AA}$  break. Other than the change of using a different optical band, the SpARCS algorithm is identical to that presented in Muzzin et al. (2008) and we refer to that paper for further details of the cluster finding technique.

After the first semester of  $z'$  observations were complete there were  $\sim 14 \text{ deg}^2$  of data with both  $z'$  and  $3.6\mu\text{m}$  data. From this area we selected two rich cluster candidates, both from the ELAIS-N2 field with red-sequence photometric redshifts<sup>15</sup> of  $z > 1.2$  for spectroscopic followup. These two cluster candidates, SpARCS J163435+402151 (R.A.: 16:34:35.0, Decl:+40:21:51.0), and SpARCS J163852+403843 (R.A.:16:38:52.0, Decl:+40:38:43.0), have richnesses, parameterized by  $B_{gc,R}$ , of  $1053 \pm 278 \text{ Mpc}^{1.8}$  and  $988 \pm 270 \text{ Mpc}^{1.8}$ , respectively. For a discussion of  $B_{gc}$  and  $B_{gc,R}$  as cluster richness estimates see Yee & Lopez-Cruz (1999), and Gladders & Yee (2005). Based on the empirical calibration of  $B_{gc}$  vs.  $M_{200}$  determined by Muzzin et al. (2007) in the K-band for the CNOC1 clusters at  $z \sim 0.3$ , this implies  $M_{200} = 5.7 \times 10^{14} M_{\odot}$  and  $5.1 \times 10^{14} M_{\odot}$  for SpARCS J163435+402151 and SpARCS J163852+403843, respectively. Although Muzzin et al. (2007) found there is a fairly large scatter in the  $B_{gc}$  vs.  $M_{200}$  relation, the high richnesses imply that these candidates are likely to be massive, high-redshift systems.

### 4. SPECTROSCOPIC DATA

Multislit nod-and-shuffle (N&S) spectroscopy of galaxies in SpARCS J163435+402151, and SpARCS J163852+403843 were obtained using GMOS-N on Gemini as part of the program GN-2007A-Q-17. We used the R150 grating blazed at  $7170\text{\AA}$  with  $1''$  width slits. This provided a resolving power of  $R = 631$  which corresponds to a resolution of  $\sim 11\text{\AA}$ , or  $\sim 250 \text{ km s}^{-1}$  at the estimated redshift of the clusters. For all observations we used  $3''$  long microslits, corresponding to roughly four seeing-disks, allowing a two seeing-disk spacing between the nod positions. We observed three masks for SpARCS J163435+402151 and four masks for SpARCS J163852+403843. One mask for each of the clusters was observed in “micro-shuffle” mode, but the majority were observed in “band-shuffle” mode. All masks were observed using the RG615 filter which blocks light blueward of  $6150\text{\AA}$  so that multiple tiers of slits could be used.

Unlike micro-shuffle where the shuffled charge is stored directly adjacent to the slit location, band-shuffle shuffles the charge to the top and bottom third of the chips for

storage. While technically it is the least-efficient N&S mode in terms of usable area for observations (only the central  $1.7'$  of the total  $5'$  FOV can be used) it is extremely efficient for observations of high-redshift clusters because it allows the microslits to be packed directly beside each other in the cluster core with no requirement for additional space for storing the shuffled charge. In band-shuffle mode we were typically able to locate between 20-26 slits, including three alignment stars, per mask in the central  $1.7'$  around the cluster. At  $z \sim 1.2$  the  $1.7'$  FOV corresponds to a diameter of 850 kpc, roughly the projected size of a massive cluster.

Slits were placed on galaxies with priorities in the following order: Priority 1, galaxies with colors  $\pm 0.6$  mag from the red-sequence and  $3.6\mu\text{m} < 16.9$ . Priority 2, galaxies with colors  $\pm 0.6$  mag from the red-sequence,  $3.6\mu\text{m} > 16.9$  and  $z' < 23.5$ . Priority 3, galaxies with colors  $> 0.6$  bluer than the red-sequence, but  $< 1.0$  mag bluer and  $3.6\mu\text{m} > 16.9$  and  $z' < 23.5$ . Priority 4, same as priority 3 but for galaxies with colors bluer than the red-sequence by 1.0-1.4 mag. Priority 5: all galaxies with  $23.5 < z' < 24.5$ . Roughly speaking, Priorities 1 through 4 can be described as bright red-sequence, faint red-sequence, blue cloud, and extreme blue cloud galaxies, respectively.

For each mask we obtained a total of 3 hrs of integration time by combining six exposures with 30 mins of integration time. The six frames were obtained using 15 nod cycles of 60s integration time per cycle. Each of the 6 exposures was offset by a few arcseconds using the on-chip dithering option.

#### 4.1. Data Reduction

Data were reduced using the GMOS IRAF package. We subtracted a bias and N&S dark from each frame. The N&S darks are taken using the same exposure times and using the same charge shuffling routine as the science observations, but with the shutter closed. Regions with poor charge transfer efficiency cause electrons to become trapped during the repeated charge shuffling used in the observations. Such charge traps can be identified and corrected using dark frames taken with the same N&S settings. Images were registered using bright sky lines and sky subtracted using the complementary storage area using the “gnsskysub” task. Final mosaics are made by coadding the sky subtracted images.

One dimensional spectra were extracted using the iGDDS software (Abraham et al. 2004). Wavelength calibration for each extracted spectrum was performed using bright sky lines from the unsubtracted image, also with the iGDDS software. Wavelength solutions typically have an rms  $< 0.5\text{\AA}$ . We determined a relative flux calibration curve using a long slit observation of the standard star EG131.

Redshifts were determined interactively for each spectrum by comparing with the templates available in iGDDS. Most of the redshifts were identified using the early-, intermediate-, and late-type composite spectra from the Gemini Deep Deep Survey (Abraham et al. 2004). The final redshifts was determined using the average redshift from all absorption and emission lines that were detected. The vast majority of redshifts were determined by identifying the [OII]  $3727\text{\AA}$ -doublet emission

<sup>15</sup> Based on a  $z_f = 2.8$  single-burst Bruzual & Charlot (2003) model

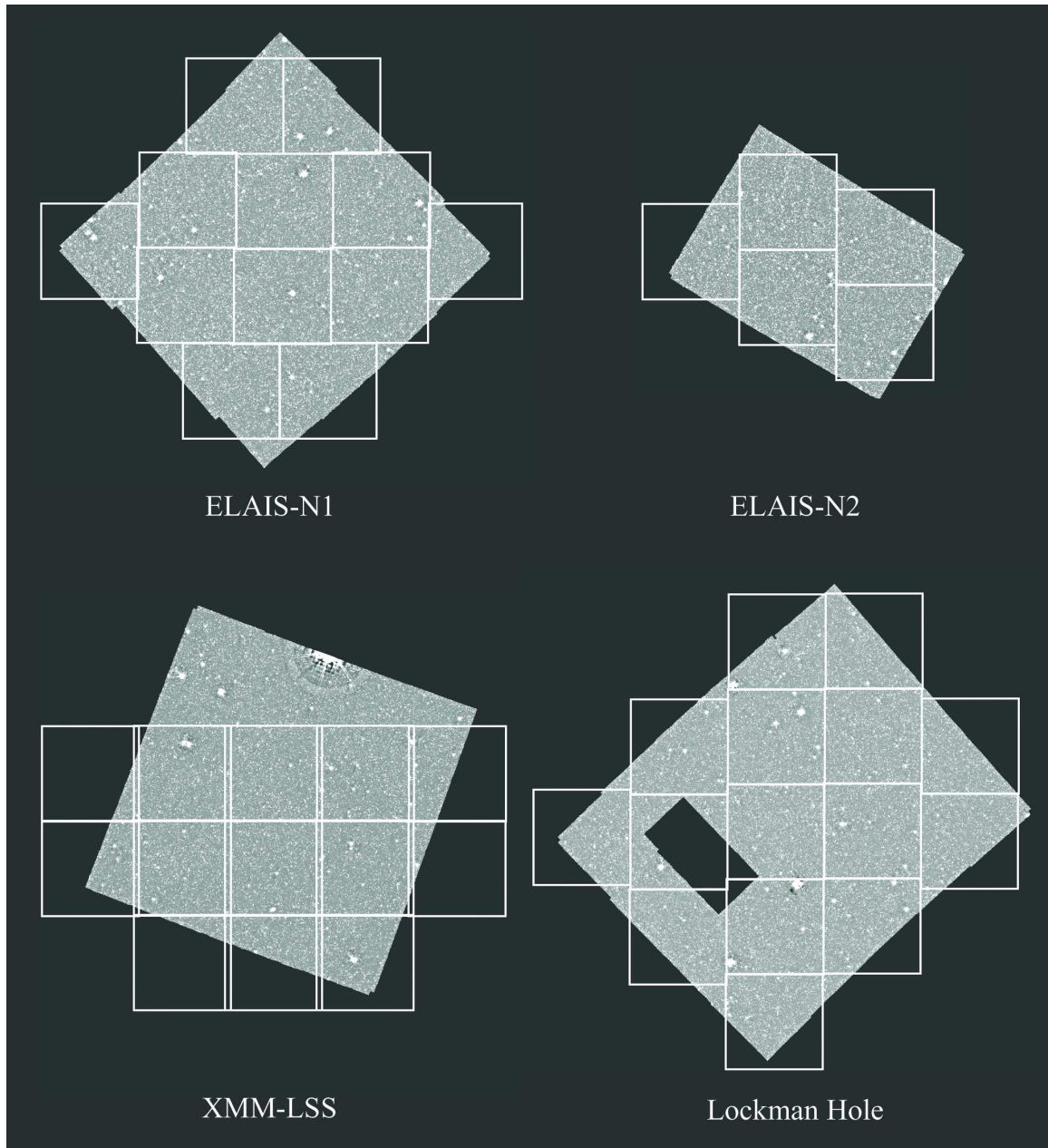


FIG. 1.— The  $3.6\mu\text{m}$  mosaics for the four SWIRE fields observable from the northern hemisphere. The location of the SpARCS  $z'$ -band CFHT/MegaCam pointings are overplotted as white boxes. Each MegaCam pointing covers  $\sim 1 \text{ deg}^2$ . The observations of the XMM-LSS field were obtained as part of the CFHTLS-wide survey. Excluding areas masked by bright stars and missed by MegaCam chip gaps there are  $28.3 \text{ deg}^2$  with both  $z'$  and  $3.6\mu\text{m}$  observations in the northern fields that can be used for cluster finding.

line (which is not resolved at our resolution), or the Calcium II H+K absorption lines. Many of the spectra also show the Balmer series lines. We list the spectroscopic members of SpARCS J163435+402151 and SpARCS J163852+403843 in Tables 1 and 2, and the spectroscopically confirmed foreground/background galaxies in Tables 3 and 4. We also plot examples of some cluster galaxy spectra in Figures 2 and 3. R,  $z'$ , and  $3.6\mu\text{m}$  color composites of the two clusters are shown in Figures 4 and 5. The white squares denote the spectroscopically confirmed cluster members and the green squares denote the spectroscopically confirmed foreground/background galaxies.

## 5. CLUSTER VELOCITY DISPERSIONS

For both clusters there are a sufficient number of redshifts to determine a velocity dispersion ( $\sigma_v$ ) and therefore a dynamical mass. Our  $\sigma_v$ 's are determined using the method detailed in Blindert (2006). Briefly, we make a rejection of near-field non-cluster members using a modified version of the Fadda et al. (1996) shifting-gap procedure. This method uses both the position and velocity of galaxies to reject interlopers. In Figure 6 we plot the relative velocities of the cluster galaxies as a function of projected radius. Two galaxies in SpARCS J163435+402151 are rejected as near-field interlopers and three are rejected in SpARCS J163852+403843. The rejected galaxies are plotted as crosses in Figure 6 and

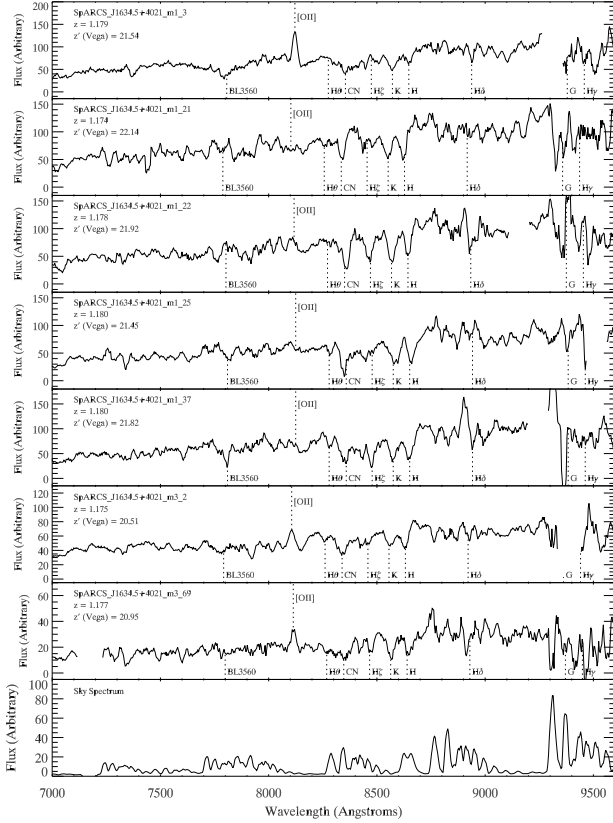


FIG. 2.— Spectra for a subsample of seven galaxies in the cluster SpARCS J163435+402151. The spectra have been smoothed with a 7-pixel boxcar so the sampling matches the instrumental resolution.

TABLE 1  
SPECTROSCOPIC CLUSTER MEMBERS IN SPARCS  
J163435+402151

ID	R.A. J2000 (Deg.)	Decl. J2000 (Deg.)	$z'$ Mag Vega	$z_{spec}$
Mask 1				
3	248.6589	40.35303	21.54	1.179
5	248.6497	40.36148	21.58	1.181
6	248.6467	40.36418	20.95	1.166
21	248.6513	40.35238	22.14	1.174
22	248.6605	40.35474	21.91	1.178
25	248.6510	40.35855	21.44	1.180
28	248.6605	40.36132	22.19	1.182
34	248.6527	40.36477	22.78	1.182
37	248.6496	40.36696	21.82	1.180
41	248.6459	40.36841	21.97	1.185
45	248.6440	40.37413	22.14	1.187
3027	248.6546	40.35461	21.59	1.181
Mask 2				
20	248.5991	40.34870	23.10	1.170
27	248.6548	40.35104	22.23	1.164
36	248.6171	40.36649	22.36	1.184
57	248.6700	40.39159	22.80	1.176
Mask 3				
2	248.6584	40.34934	20.50	1.175
38	248.6474	40.36152	21.67	1.178
69	248.6669	40.39132	21.89	1.178

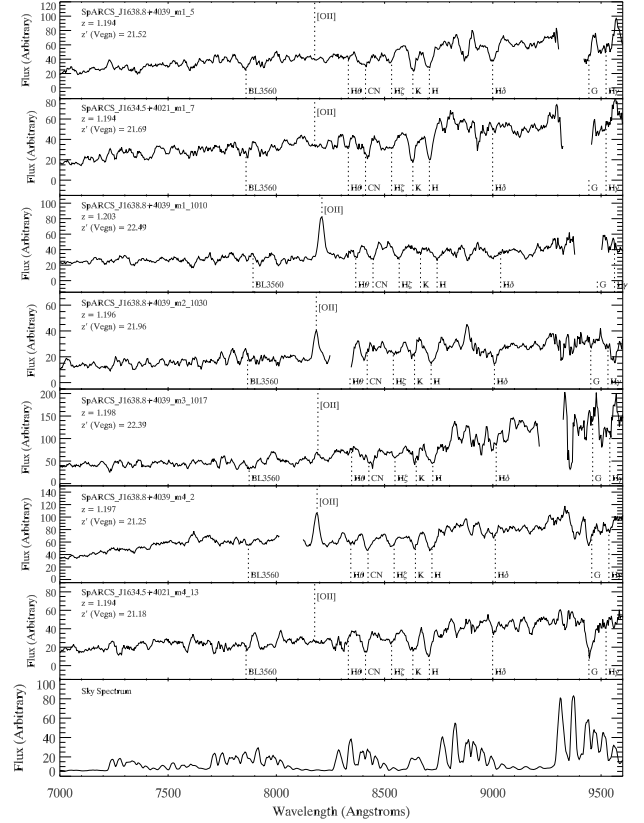


FIG. 3.— Same as Figure 2 but for galaxies in the cluster SpARCS J163852+403843.

are not used in computing the mean redshift of the cluster or  $\sigma_v$ . Once outliers are rejected the redshift of the clusters is determined using the remaining galaxies. The spectroscopic redshift of the clusters is 1.1798 and 1.1963 for SpARCS J163435+40215 and SpARCS J163852+403843, respectively.

The  $\sigma_v$ 's are determined using the “robust” estimator suggested by Beers et al. (1990) and Girardi et al. (1993). The robust estimator is simply the biweight estimator for systems with  $> 15$  members, and the gap-per estimator for systems with  $< 15$  members. As discussed in those papers and Blindert (2006) these estimators are more robust than standard deviations as they are less sensitive to outliers, which may still persist even after the initial shifting-gap rejection. Using the “robust” estimator, SpARCS J163435+402151 and SpARCS J163852+403843 have  $\sigma_v = 490 \pm 140 \text{ km s}^{-1}$  and  $650 \pm 160 \text{ km s}^{-1}$ , respectively, where the errors have been determined using Jackknife resampling of the data.

We estimate the dynamical mass using  $M_{200}$ , the mass contained within  $r_{200}$ , the radius at which the mean interior density is 200 times the critical density ( $\rho_c$ ). We use the equation,

$$M_{200} = \frac{4}{3} \pi r_{200}^3 \cdot 200 \rho_c, \quad (1)$$

with the dynamical estimate of  $r_{200}$  from Carlberg et al. (1997),

$$r_{200} = \frac{\sqrt{3}\sigma}{10H(z)}, \quad (2)$$

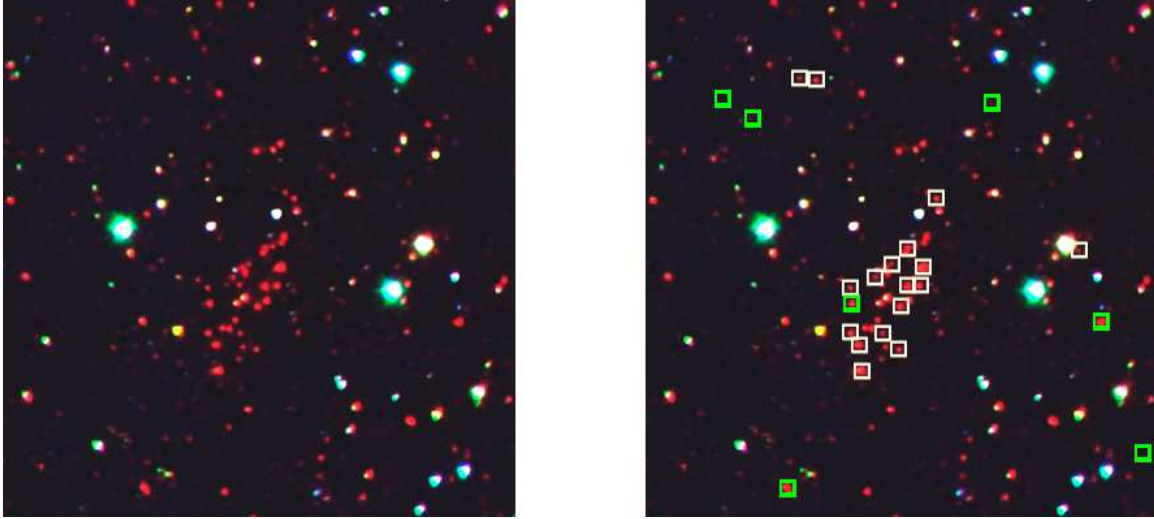


FIG. 4.— Left:  $Rz'3.6\mu\text{m}$  color composite of the cluster SpARCS J163435+402151 at  $z = 1.1798$ . The  $R$  and  $z'$  images have been convolved to match the  $3.6\mu\text{m}$  PSF. The FOV of the image is  $\sim 3.5'$  across. Right: Same as left panel but with spectroscopically confirmed cluster members marked as white squares and spectroscopically confirmed foreground/background galaxies marked as green squares.

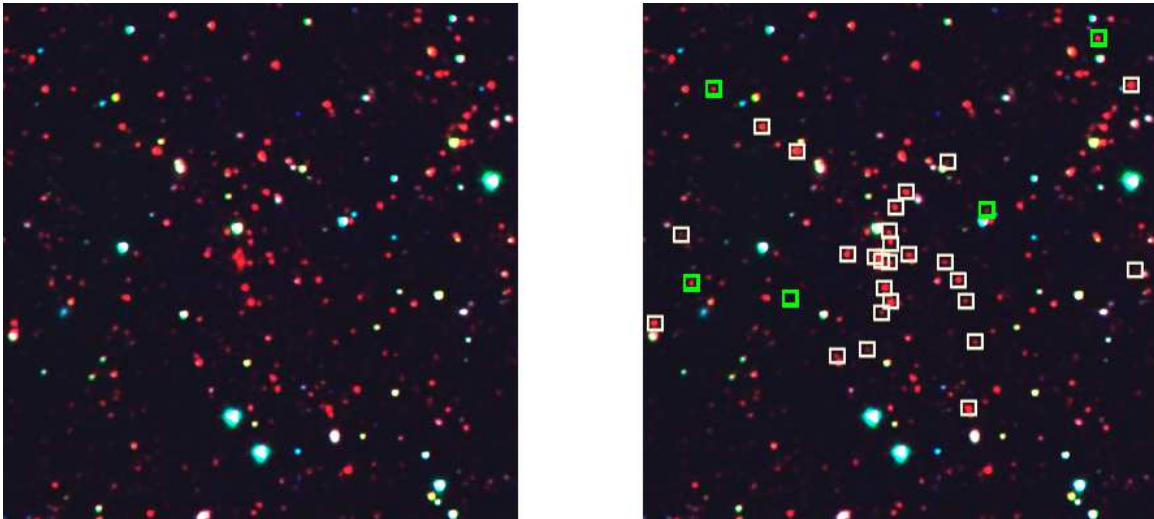


FIG. 5.— As Figure 4, but for the cluster SpARCS J163852+403843 at  $z = 1.1963$ . The FOV of the images is  $\sim 4.5'$  across.

where  $H(z)$  is the Hubble constant at the redshift of the cluster. From these relation we derive  $r_{200} = 0.62 \pm 0.18$  Mpc, and  $0.82 \pm 0.20$  Mpc for SpARCS J163435+402151 and SpARCS J163852+403843, respectively. From Equation 2, these imply  $M_{200} = (1.0 \pm 0.9) \times 10^{14} M_{\odot}$  and  $(2.4 \pm 1.8) \times 10^{14} M_{\odot}$  for SpARCS J163435+402151 and SpARCS J163852+403843, respectively.

## 6. DISCUSSION

### 6.1. Red-sequence Photometric Redshifts

In Figure 7 we plot the  $z' - 3.6\mu\text{m}$  vs.  $3.6\mu\text{m}$  color magnitude relation for galaxies at projected radii ( $R$ )  $< 550$  kpc in the fields of both clusters. Spectroscopically confirmed members and confirmed foreground/background galaxies are plotted as red and blue diamonds, respectively. The dotted line in both panels is the best fit line with the slope fixed at zero, to the spectroscopically confirmed members. These lines indicate that the red-sequence galaxies have  $z' - 3.6\mu\text{m}$  colors of 4.77

and 4.82 for SpARCS J163435+402151 and SpARCS J163852+403843, respectively. Using a solar metallicity, Bruzual & Charlot (2003) simple stellar population (SSP) with a  $z_f = 4.0$  these colors imply photometric redshifts of 1.19 and 1.20, in excellent agreement with the spectroscopic redshifts. At  $z \sim 1.2$ , the red-sequence photometric redshifts do not depend strongly on the chosen  $z_f$ . If we instead use a  $z_f = 2.8$  SSP, the red-sequence color would predict redshifts of 1.21 and 1.24, and for a  $z_f = 10.0$  SSP it would predict redshifts of 1.13 and 1.15. However, the color differences between all these models at fixed redshift are small ( $< 0.1$  mag), and so it is not possible to distinguish between different formation epochs without more data. Still, the close agreement between the red-sequence photometric redshift derived using a reasonable  $z_f$  and the spectroscopic redshift is encouraging for the use of red-sequence photometric redshifts for clusters at  $z > 1$ .

### 6.2. Mass vs. Richness

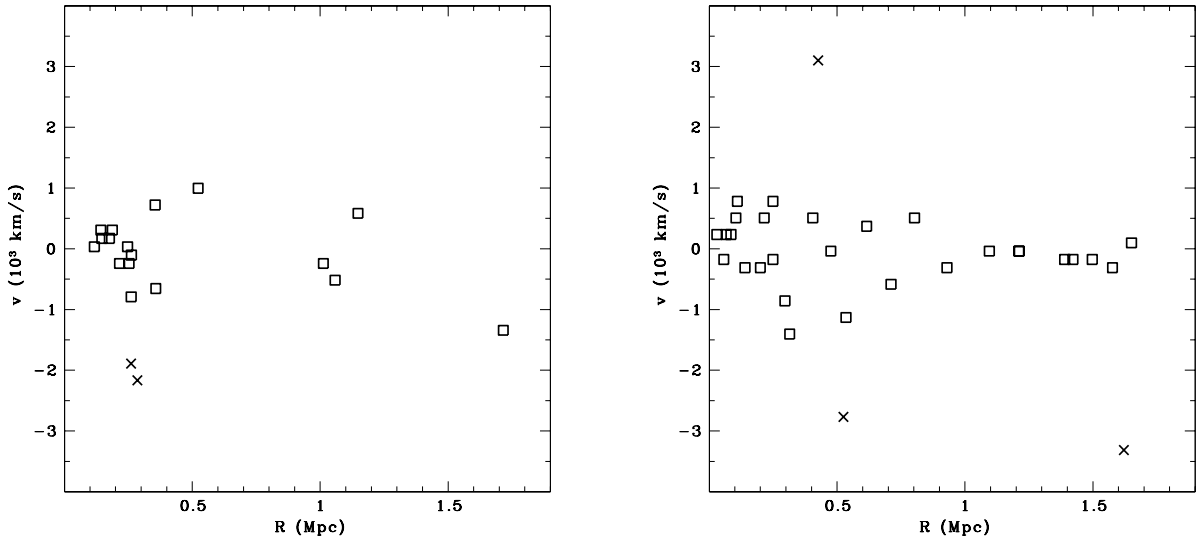


FIG. 6.— Left Panel: Galaxy velocities relative to the cluster mean velocity as a function of radius for SpARCS J163435+402151. Right Panel: Same as left panel but for SpARCS J163852+403843. Galaxies marked with an “x” are more likely to be near-field objects than members of the cluster and are not used in the computation of the velocity dispersion.

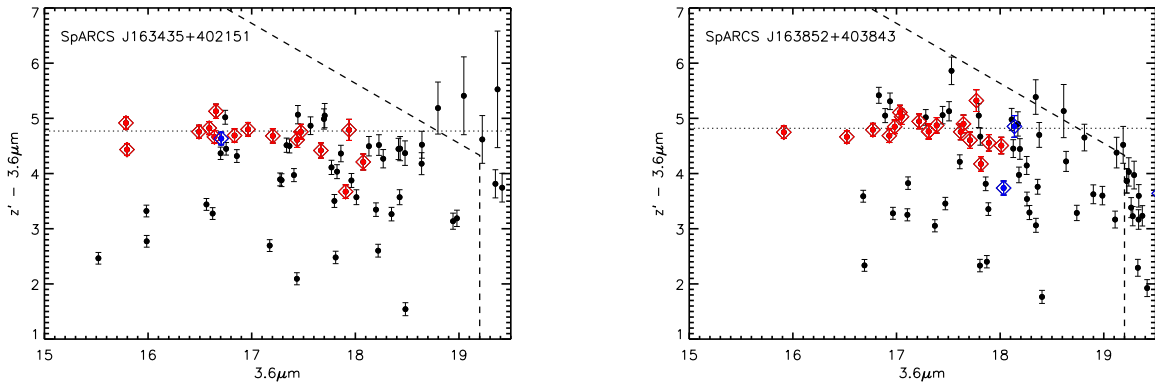


FIG. 7.— Left Panel:  $z' - 3.6\mu\text{m}$  vs.  $3.6\mu\text{m}$  color magnitude diagram for galaxies at  $R < 550$  kpc in the field of the cluster SpARCS J163435+402151. Spectroscopically confirmed cluster members and foreground/background galaxies are plotted as red and blue diamonds, respectively. The dotted line is the best fit line to the confirmed cluster members with the slope fixed at zero. Right Panel: Same as left panel but for SpARCS J163852+403843.

Both clusters have lower masses than predicted by their richness by factors of  $\sim 6$  and  $2$  for SpARCS J163435+402151 and SpARCS J163852+403843, respectively, although due to the large error bars the differences are only significant at  $\sim 1$  and  $2\sigma$ , respectively. Whether this represents a redshift evolution in the  $B_{gc} - M_{200}$  scaling relation, or is simply a richness-selected Eddington bias<sup>16</sup> is impossible to determine using only two clusters. Both Gilbank et al. (2007) and Andreon et al. (2007) found that for a small sample of clusters at  $z \sim 1$  the cluster richnesses were still consistent with their velocity dispersions based on relations calibrated at lower redshift, although both parameters have large uncertainties in their measurements. More clusters with well-determined  $\sigma_v$  and  $B_{gc}$  will be needed to test if the

<sup>16</sup> We followed up two of the richest clusters in our early dataset. The cluster mass function is steep at high redshift and low mass systems greatly outnumber high mass systems. Due to scatter in the mass-richness relation lower mass systems with abnormally high richnesses may be more common than truly massive systems.

cluster scaling relations at  $z > 1$  are similar to those at lower redshift.

## 7. SUMMARY

We have presented a brief summary of observations for the northern component of the SpARCS survey. Using Gemini N&S spectroscopy we confirmed two rich cluster candidates at  $z \sim 1.2$  selected from early survey data. We find that the photometric redshifts from the color of the cluster red-sequence agree extremely well with the spectroscopic redshifts. Both clusters have a smaller  $M_{200}$  than would be expected from their richness if we use the  $B_{gc} - M_{200}$  scaling relation calibrated at  $z \sim 0.3$ . Whether this represents a true evolution in the cluster scaling relations at  $z > 1.2$  or is simply a selection bias will require well-determined  $M_{200}$  for a larger sample of clusters.

Overall, the confirmation of both SpARCS J163435+402151 and SpARCS J163852+403843 as *bona fide* massive clusters at  $z > 1$  provide strong

TABLE 2  
SPECTROSCOPIC CLUSTER MEMBERS IN SPARCS  
J163852+403843

ID	R.A. J2000 (Deg.)	Decl. J2000 (Deg.)	$z'$ Mag Vega	$z_{spec}$
Mask 1				
5	249.7132	40.63952	21.51	1.194
7	249.7144	40.64159	21.68	1.194
8	249.7152	40.64527	21.41	1.195
1007	249.6974	40.63383	22.50	1.199
1010	249.7151	40.63804	22.48	1.202
1016	249.7006	40.64276	22.20	1.200
1025	249.7137	40.64952	22.46	1.200
1028	249.7104	40.65532	21.96	1.190
1031	249.7029	40.65968	22.85	1.176
3026	249.6668	40.64420	22.73	1.195
Mask 2				
1018	249.7032	40.64533	22.67	1.186
1020	249.7099	40.64631	22.39	1.202
1024	249.7135	40.64828	22.24	1.198
1026	249.7126	40.65311	22.26	1.200
1030	249.7581	40.63628	21.95	1.195
2016	249.6610	40.65976	22.22	1.197
Mask 3				
1017	249.7136	40.64511	22.38	1.198
1019	249.7163	40.64602	22.29	1.198
2009	249.7236	40.63171	22.10	1.188
4029	249.7619	40.65497	23.67	1.195
Mask 4				
2	249.6947	40.61541	21.24	1.196
3	249.6986	40.62432	21.73	1.200
10	249.7314	40.66114	21.25	1.192
11	249.7378	40.66462	21.72	1.194
13	249.6680	40.67089	21.17	1.194
2014	249.7532	40.64920	22.58	1.196
2030	249.7049	40.68847	21.87	1.175
1012	249.6992	40.63979	23.06	1.196
1021	249.7217	40.64632	21.90	1.195
3019	249.7189	40.63320	23.17	1.219
3046	249.7509	40.68401	22.05	1.172

TABLE 3  
SPECTROSCOPIC FOREGROUND/BACKGROUND GALAXIES  
IN FIELD OF SPARCS J163435+402151

ID	R.A. J2000 (Deg.)	Decl. J2000 (Deg.)	$z'$ Mag Vega	$z_{spec}$
Mask 1				
4	248.6129	40.35610	20.89	1.108
26	248.6600	40.35898	21.38	1.004
31	248.6042	40.36213	21.66	1.105
45	248.6823	40.38687	23.64	0.925
Mask 2				
23	248.60280	40.33815	23.79	1.337
24	248.60710	40.33762	24.05	1.255
Mask 3				
1	248.67280	40.33252	21.16	1.348
15	248.65750	40.33183	21.32	0.780
65	248.67920	40.38581	23.45	1.108
67	248.63340	40.38773	23.05	0.811

evidence that the red-sequence technique is an effective

and efficient method for detecting clusters at  $z > 1$  (see also Wilson et al. 2008 who present a confirmed  $z = 1.34$  cluster from the southern component of the SPARCS survey). The complete SPARCS catalogue contains *hundreds* of cluster candidates at  $z > 1$  and promises to be one of the premier data sets for the study of cluster galaxy evolution at  $z > 1$ .

TABLE 4  
SPECTROSCOPIC FOREGROUND/BACKGROUND GALAXIES  
IN FIELD OF SPARCS J163852+403843

ID	R.A. J2000 (Deg.)	Decl. J2000 (Deg.)	$z'$ Mag Vega	$z_{spec}$
Mask 1				
3021	249.7659	40.63502	22.14	0.670
Mask 2				
3024	249.7503	40.64119	23.61	0.875
4020	249.7305	40.63887	23.98	1.391
4030	249.7666	40.65555	23.56	0.776
Mask 3				
3034	249.6953	40.65273	21.96	1.393
3036	249.6603	40.65813	23.47	1.386
Mask 4				
1	249.7320	40.60904	22.10	0.963
12	249.6992	40.66802	20.96	0.784
2003	249.6765	40.60412	22.44	1.017
2024	249.7496	40.67251	23.50	0.848
2026	249.6744	40.67759	21.46	0.771
3004	249.7519	40.60677	21.44	0.768
3041	249.7611	40.67033	21.17	0.784

Based on observations obtained with MegaPrime/MegaCam, a joint project of CFHT and CEA/DAPNIA, at the Canada-France-Hawaii Telescope (CFHT) which is operated by the National Research Council (NRC) of Canada, the Institut National des Sciences de l'Univers of the Centre National de la Recherche Scientifique (CNRS) of France, and the University of Hawaii. This work is based in part on data products produced at TERAPIX and the Canadian Astronomy Data Centre as part of the Canada-France-Hawaii Telescope Legacy Survey, a collaborative project of NRC and CNRS.

Based on observations obtained at the Gemini Observatory, which is operated by the Association of Universities for Research in Astronomy, Inc., under a cooperative agreement with the NSF on behalf of the Gemini partnership: the National Science Foundation (United States), the Science and Technology Facilities Council (United Kingdom), the National Research Council (Canada), CONICYT (Chile), the Australian Research Council (Australia), Ministerio da Ciencia e Tecnologia (Brazil) and SECYT (Argentina)

This work is based in part on observations made with the Spitzer Space Telescope, which is operated by the Jet Propulsion Laboratory, California Institute of Technology under a contract with NASA.

#### REFERENCES

- Abraham, R. G., et al. 2004, *AJ*, 127, 2455  
 Andreon, S., Valtchanov, I., Jones, L. R., Altieri, B., Bremer, M., Willis, J., Pierre, M., Quintana, H. 2005, *MNRAS*, 359, 1250  
 Andreon, S., De Propriis, R., Puddu, E., Giordano, L., Quintana, H. 2008, *MNRAS*, 383, 102  
 Balogh, M. L., Baldry, I. K., Nichol, R., Miller, C., Bower, R., & Glazebrook, K. 2004, *ApJ*, 615, L101  
 Beers, T. C., Flynn, K., & Gebhardt, K. 1990, *AJ*, 100, 32  
 Bertin, E., & Arnouts, S. 1996, *A&AS*, 117, 393  
 Blanton, M. R., Eisenstein, D., Hogg, D. W., Schlegel, D. J., Brinkmann, J. 2005, *ApJ*, 629, 143  
 Blindert, K. 2006, Ph.D. Thesis, University of Toronto  
 Bremer, M. N., et al. 2006, *MNRAS*, 371, 1427  
 Brodwin, M., et al. 2006, *ApJ*, 651, 791  
 Bruzual, G., & Charlot, S. 2003, *MNRAS*, 344, 1000



- Capak, P., Abraham, R. G., Ellis, R. G., Mobasher, B., Scoville, N., Sheth, K., Koekemoer, A. 2007, *ApJSS*, 172, 284
- Carlberg, R. G., Yee, H. K. C., & Ellingson, E. 1997, *ApJ*, 478, 462
- Cooper, M., et al. 2007, *MNRAS*, 376, 1445
- Cooper, M., et al. 2008, *MNRAS*, 383, 1058
- Croton, D., et al. 2005, *MNRAS*, 356, 1155
- Dressler, A. 1980, *ApJ*, 236, 351
- Dressler, A., et al. 1997, *ApJ*, 490, 577
- Eisenhardt, P. et al. 2008, *ApJ*, 684, 905
- Elbaz D., et al. 2007, *A&A*, 468, 33
- Fadda, D., Girardi, M., Giuricin, G., Mardirossian, F., Mezzetti, M. 1996, *ApJ*, 473, 670
- Finoguenov, A., et al. 2007, *ApJSS*, 172, 182
- Gilbank, D. G., Bower, R. G., Castander, F. J., Ziegler, B. L. 2004, *MNRAS*, 348, 551
- Gilbank, D. G., Yee, H. K. C., Ellingson, E. E., Gladders, M. D., Barrientos, L. F., & Blindert, K. 2007, *AJ*, 134, 282
- Girardi, M., Biviano, A., Giuricin, G., Mardirossian, F., Mezzetti, M. 1993, *ApJ*, 404, 38
- Gladders, M. D., & Yee, H. K. C., 2000, *AJ*, 120, 2148
- Gladders, M. D., & Yee, H. K. C. 2005, *ApJSS* 157, 1
- Gomez, P., et al. 2003, *ApJ*, 584, 210
- Goto, T., Yamauchi, C., Fujita, Y., Okamura, S., Sekiguchi, M., Smail, I., Bernardi, M., Gomez, P. L. 2003, *MNRAS*, 346, 601
- Hogg, D. W., et al. 2003, *ApJ*, 585, L5
- Hogg, D. W., et al. 2004, *ApJ*, 601, L29
- Kauffmann, G., White, S. D. M., Heckman, T. M., Menard, B., Brinchmann, J., Charlot, S., Tremonti, C., Brinkmann, J., 2004, *MNRAS*, 353, 713
- Krick, J. E., Surace, J. A., Thompson, D., Ashby, M. L. N., Hora, J. L., Gorjian, V., Yan, L. 2008, *arXiv:0807.1565*
- Lacy, M. et al. 2005, *ApJSS*, 161, 41
- Lamer, G., Hoeft, M., Kohnert, J., Schwobe, A., Storm, J. 2008, *A&A*, 487, L33
- Lewis, I., et al. 2002, *MNRAS*, 334, 673
- Lonsdale, C. J. et al. 2003, *PASP*, 115, 897
- Mullis, C. R., Rosati, P., Lamer, G., Bohringer, H., Schwobe, A., Schuecker, P., Fassbender, R. 2005, *ApJ*, 623, L85
- Muzzin, A., Yee, H. K. C., Hall, P. B., & Lin, H. 2007, *ApJ*, 663, 150
- Muzzin, A., Wilson, G., Lacy, M., Yee, H. K. C., & Stanford, S. A. 2008, *arXiv:0807.0227*
- Muzzin, A., et al. 2009, in preparation
- Park, C., Choi, Y.-Y., Vogeley, M. S., Gott, J. R., & Blanton, M. 2007, *ApJ*, 658, 898
- Pierre, M., et al. 2006, *MNRAS*, 372, 591
- Poggianti, B. M., et al. 2008, *ApJ*, 684, 888
- Postman, M., et al. 2005, *ApJ*, 623, 721
- Romer, A. K., Viana, P. T. P., Liddle, A. R., Mann, R. G. 2001, *ApJ*, 547, 594
- Smith, G. P., Treu, T., Ellis, R. S., Moran, S. M., & Dressler, A. 2005, *ApJ*, 620, 78
- Stanford, S. A., et al., 2005, *ApJ*, 634, L129
- Stanford, S. A., et al. 2006, *ApJ*, 646, L13
- van Breukelen, C., et al. 2007, *MNRAS* 382, 971
- Valtchanov, I., et al. 2004, *A&A*, 423, 75
- Wilson, G., et al. 2008, *ApJ*, submitted *arXiv:0810.0036*
- Yee, H. K. C., Gladders, M. D., Gilbank, D. G., Majumdar, S., Hoekstra, H., & Ellingson, E., 2007, *astro-ph 0701839*
- Yee, H. K. C., & Lopez-Cruz, O., 1999, *AJ*, 117, 1985
- Yee, H. K. C., Gladders, M. D., Gilbank, D. G., Majumdar, S., Hoekstra, H., Ellingson, E. 2007, *ASP Conf. Ser.* 379, 103
- Zatloukal, M., Roser, H.-J., Wolf, C., Hippelein, H., Falter, S. 2007, *A&A*, 474, L5